

# Electronic structure near an impurity and terrace on the surface of a 3-dimensional topological insulator

Qiang-Hua Wang<sup>1</sup>, Da Wang<sup>1</sup>, and Fu-Chun Zhang<sup>2</sup>

<sup>1</sup>National Laboratory of Solid State Microstructures and Department of Physics, Nanjing University, Nanjing 210093, China and

<sup>2</sup>Department of Physics, The University of Hong Kong, Pokfulam Road, Hong Kong, China

Motivated by recent scanning tunneling microscopy experiments on surfaces of  $\text{Bi}_2\text{Se}_3$  [7, 10] and  $\text{Bi}_2\text{Te}_3$  [8, 9] we theoretically study the electronic structure of a 3-dimensional (3D) topological insulator in the presence of a local impurity or a domain wall on its surface using a 3D lattice model. While the local density of states (LDOS) oscillates significantly in space at energies above the bulk gap, the oscillation due to the in-gap surface Dirac fermions are very weak. The extracted modulation wave number as a function of energy satisfies the Dirac dispersion for in-gap energies and follows the border of the bulk continuum above the bulk gap. We have also examined analytically the effects of the defects by using a pure Dirac fermion model for the surface states and found that the LDOS decays asymptotically faster at least by a factor of  $1/r$  than that in normal metals, consistent with the results obtained from our lattice model.

## I. INTRODUCTION

A three-dimensional (3D) topological insulator (TI) is a time-reversal invariant system with bulk gap but support massless Dirac fermions with coupled spin and momentum on the surface. [1, 2] The existence and the (odd) number of Dirac cones of the massless dispersion are protected by the  $Z_2$  topology of the bulk band structure. [3] Recent first principle calculation reveals that  $\text{Sb}_2\text{Te}_3$ ,  $\text{Bi}_2\text{Te}_3$  and  $\text{Bi}_2\text{Se}_3$  crystals are potential topological insulators. [4] Quite excitingly angle-resolved photoemission (ARPES) experiments have confirmed many of the proposed topological insulators. [5] Before harvesting the novel properties of TIs, [6] an interesting question is how robust the surface Dirac fermions are against imperfections, such as local and extended impurities. This issue is made interesting and challenging by recent scanning tunnelling microscopy (STM) measurements. [7-10] It is observed that while local impurities are seen to induce local density of states (LDOS) oscillation, [9] surprisingly the domain wall (a terrace on the surface) does not seem to induce LDOS oscillations for energies within the bulk gap. [7, 8, 10]

We investigate the above issue by a model lattice hamiltonian for a 3-dimensional TI. The main results are as follows. 1) We obtain the surface Green's function and therefore the spectral function for the surface states. The contributions from surface Dirac fermions and the bulk extended states are clearly identified. 2) For an upper terrace on the surface, we find the LDOS oscillation is vanishingly weak for energies below the bulk gap, where Dirac fermions are best defined. The oscillation is significant above, but it can be clearly ascribed to the contributions from the bulk extended states near the bottom of the conduction band. The numerical phenomenology is in nice agreement with the experiment. [7, 8, 10] On the other hand, the LDOS oscillation on the lower terrace is globally weak. The asymmetry of the terraces can be attributed to the difference in the effective scattering

mechanism. 3) For a local unitary impurity on a flat surface, we find LDOS oscillations at all energies, although it is relatively weaker below. 4) Combining both terraces and local impurities, we extract from the LDOS oscillations the energy dependence of the modulation wave number  $2k_\parallel$ . For  $\epsilon < 0$  the dispersion ( $\epsilon$  vs.  $k_\parallel$ ) coincides with that of surface Dirac fermions, while for  $\epsilon > 0$  it is actually related to the bulk extended states. The above numerical results combine to support the robustness of surface Dirac fermions. 5) For comparison, we substantiate analytical results using pure Dirac fermion models subject to impurity scattering. Asymptotically, the oscillation in LDOS, if present at all, has an energy dependent wave number  $2k_\parallel$ , where  $k_\parallel$  is the on-shell momentum, and decays faster by a factor of  $1/r$  than that for usual fermions. In particular, a hard domain wall in 2D Dirac models does not lead to any LDOS oscillations at all. These are in qualitative agreement with the numerical results for the full 3d model. However, we do find and discuss differences between surface and pure Dirac fermions in connection to the nature of the wave functions.

The rest of the paper is organized as follows. We discuss the surface states using a 3D lattice model in sections II-IV, where a perfect surface, a terrace and a local impurity are discussed, respectively. Sec.V contains analytical results using pure Dirac models. We summarize and provide remarks in connection to experiments in Sec.VI.

## II. SURFACE STATES IN A LATTICE MODEL OF TOPOLOGICAL INSULATORS

We start with a 3D lattice model for topological insulators. The hamiltonian is given by  $H = \sum_{\mathbf{k}} \sum_{\alpha\beta} h_{\alpha\beta}(\mathbf{k}) c_{\alpha}^\dagger c_{\beta}$ , where  $c_{\alpha}$  is a 4-spinor,  $\mathbf{k}$  is the lattice momentum, and

$$h_{\mathbf{k}} = \left[ m \sum_b \gamma_b (2t_b (\cos k_b - 1)) \right]_0 + \sum_b 2t_b \sin k_b \gamma_b; \quad (1)$$

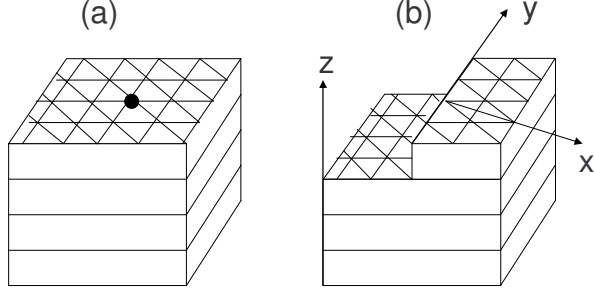


FIG. 1: Schematic plot of a topological insulator with layered hexagonal structure, and a local impurity (filled circle) (a) and (upper and lower) terraces (b) on the surface. Here  $x$ ,  $y$  and  $z$  denote the orthogonal axes, and the normal direction of the terrace edge is along  $x$ . The inter-layer hopping is along the vertical direction  $z$ .

where  $m$  is a parameter controlling the bulk gap,  $t_b$  is the hopping amplitude along a bond  $b$ ,  $k_b = k \cdot \hat{b}$ , and  $\hat{b} = (\hat{x} + \hat{y} + \hat{z})/\sqrt{3}$ . Here  $\hat{x}$ ,  $\hat{y}$  and  $\hat{z}$  are three orthogonal unit vectors,  $\hat{b}$  is the unit vector along  $b$ , and  $\gamma_n$ 's (for  $n = 0, 1, 2, 3$ ) are Hermitian Dirac matrices that satisfy the Clifford algebra  $\{\gamma_n, \gamma_m\} = 2\delta_{nm}$ . Explicitly we take  $\gamma_1 = \sigma_x$ ,  $\gamma_2 = \sigma_y$ ,  $\gamma_3 = \sigma_z$  and  $\gamma_0 = \gamma_1\gamma_2\gamma_3$ , where  $\sigma_i$  are Pauli matrices ( $\sigma_0$  is the unit matrix). However, the general conclusion does not rely on the parameterization of the Dirac matrices. Decomposing  $h_k$  as  $h_k = \sum_b h_b e^{ik \cdot b}$ , one sees that the bulk dispersion is given by  $\epsilon = E_k$  with  $E_k = \sqrt{m^2 + \sum_b t_b^2 \sin^2 k_b}$ . We define  $m$  in  $E_k$  as the bulk gap, which is assumed nonzero. We specify to a layered hexagonal lattice illustrated in Figs. 1 (the impurities are considered in the next section), as would be relevant to the experiments. [7–10] For simplest purposes we consider a nearest-neighbor tight-binding model and set  $2t_n = 1$  and  $m = 0$  henceforth. In this case  $\epsilon = 1$ .

We use a recursion method to obtain the surface Green's function. In the presence of open surfaces normal to  $z$ , the planar momentum  $k_{\parallel} = (k_x, k_y)$  is still a good quantum number. For each  $k_{\parallel}$  the Hamiltonian can be decomposed formally into intra-layer part  $\sum_n \gamma_n h_{k_{\parallel}}^{2d} \gamma_n$  and inter-layer part  $\sum_n \gamma_n h_z \gamma_{n+1} + h.c.$  where  $n$  is the layer index,

$$h_{k_{\parallel}}^{2d} = \sum_{b \in \hat{z}} [m + 2t_b \sum_{b \in \hat{z}} 2t_b (\cos k_b - 1)]_0 + \sum_{b \in \hat{z}} 2t_b \sin k_b \gamma_b;$$

and  $h_z = t_z(\gamma_0 + i\gamma_3)$  before setting our parameterization. Denote  $g = 1/(zI - h_{k_{\parallel}}^{2d})$  as the Green's function for an isolated layer (here  $z = \epsilon + i0^+$  for retarded Green's function, and  $I$  is the  $4 \times 4$  unit matrix), the surface Green's function for an  $N$ -layer lattice is given by, recur-

sively,

$$G_N^{-1} = g^{-1} - h_z^\dagger G_{N-1} h_z; \quad (2)$$

starting with  $G_1 = g$ . Amazingly it is able to prepare samples with a series of layers in recent experiments. [11] In this case the recursion method is particularly useful to reveal the evolution of the surface states as the sample thickness increases. However, in this paper, we are only interested in infinite-layer lattices, for which  $G^{-1} = g^{-1} - h_z^\dagger G h_z$  holds for  $G = G_1$ .

The spectral function for the surface states is given by

$$A(k_{\parallel}; \epsilon) = -\frac{1}{\pi} \text{Im Tr } G_{k_{\parallel}}; \quad (3)$$

where the planar momentum is indicated explicitly. The distribution in the momentum space is plot in Figs. 2 (a)–(d) for a series of  $\epsilon$  (only positive energies are displayed since the spectrum is particle-hole symmetric). It is seen that there is only a single dark spot at  $\epsilon = 0$ . This indicates that we have but one Dirac cone in the Brillouin zone. The spot evolves to a ring with increasing size for  $\epsilon < 1$ . For  $\epsilon > 1$  bulk continuum starts to contribute, forming doubled ring structure at  $\epsilon = 1.2$  in combination with the Dirac ring. For still higher energies, the ring structure is blurred (not shown). Since  $A(k_{\parallel}; \epsilon)$  is quite rotationally symmetric in the  $k_{\parallel}$  space for the energy window under concern (hexagonal structure shows up at higher energies), we plot it in Fig. 2 (e) (gray) along a line cut  $(k_x, 0)$ . A clear massless Dirac dispersion is seen. The bulk continuum starts at  $\epsilon = 1$  and  $k_{\parallel} = 0$ , and the outer border expands with increasing energies, while the Dirac dispersion persists for  $\epsilon > 1$  but eventually diminishes for  $\epsilon > 1.3$ . The contributions from surface Dirac fermions and bulk continuum are clearly separable. In comparison to pure Dirac models, the surface Dirac fermions have a momentum dependent spectral weight, the exact nature of which will be discussed elsewhere.

### III. TERRACES ON THE SURFACE

Experimentally terraces often appear on the surface. We assume the upper terrace is one unit-cell higher than the lower one, as in the experiment [7–10] and illustrated in Fig. 1 (b). The Green's function  $G$  on the terraces is obtained as follows. First, we map the hexagonal lattice to a square lattice. The three principle translation axes in the hexagonal lattice are mapped to the horizontal, vertical and  $45^\circ$  axes on the square lattice, for which we denote the positions in real and momentum space as  $(u; v)$  and  $(p; q)$ , respectively. Consider the top two layers. We denote

$$G_q(u) = \frac{1}{M} \sum_p G(p; q) e^{ip \cdot u} \quad (4)$$

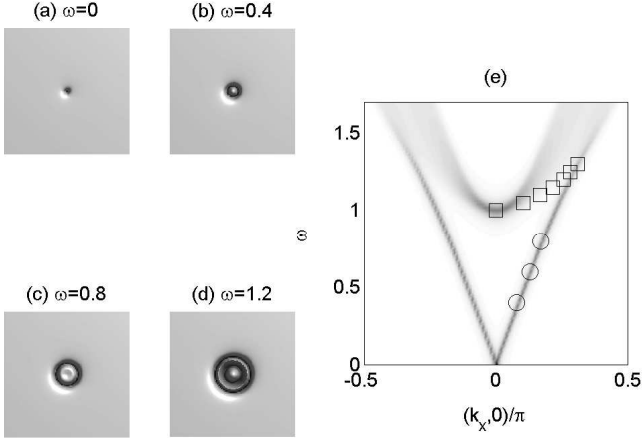


FIG. 2: (a)–(d): Intensity plot of  $A(k_{\parallel}; !)$  in the planar  $k_{\parallel}$ -space at  $! = 0, 0.4, 0.8, 1.2$ . The intensity scales with the darkness. The view field is bounded by  $2 \times 2$  (within the hexagonal Brillouine zone). Camera lighting is used to enhance the contrast. (e) Intensity plot of  $A(k_{\parallel}; !)$  along a cut  $(k_{\perp}, 0)$  (gray). The open squares and circles are extracted from LDOS oscillations in Fig.3 (b) and Fig.4, respectively.

as the  $q$ -resolved unperturbed Green's function, where  $M$  is the number of lattice sites along the  $u$ - or  $v$ -axis, and  $! = U; L$  denotes the upper or lower layer. The Green's function  $G(p; q)$  can be obtained by coupling an isolated upper layer (through  $h_z$ ) to a surface already considered in the previous section. Now setting  $m ! = 1$  for  $u = 0$  on the highest layer effectively depletes the left half of that layer, leaving the lower-left (upper-right) layer  $m$  mic of the lower (upper) terrace. The perturbed Green's function  $G$  for the top two layers can be obtained by the T-matrix formalism, [12]

$$G_q(u; u^0) = G_q(u; u^0) + \sum_{u_a, u_b} G_q^U(u; u_a) T_q(u_a; u_b) G_q^U(u_b; u^0); \quad (5)$$

where the layer index  $U$  and the condition  $u_a, u_b = 0$  indicate that the depleted region is the upper-left layer, and  $T_q$  is the  $q$ -resolved T-matrix given by  $T_q^{-1}(u_a; u_b) = G_q^U(u_a; u_b)$ . As what is required,  $G_q(u; u^0) = 0$  whenever  $u$  or  $u^0$  falls on the upper-left layer. We emphasize the Green's function obtained this way contains all effects from the bulk below the terraces. The LDOS on the terraces is given by,

$$\rho(!; u) = \frac{1}{M} \text{Im Tr} \sum_q G_q(u; u); \quad (6)$$

where  $! = L$  ( $= U$ ) for  $u < 0$  ( $u > 0$ ). Finally we map  $u$  back to the normal displacement  $x$  from the edge on the hexagonal lattice, as shown in Fig.1 (b).

The LDOS as a function of  $x$  is shown in Fig.3 (a) and (b) for the lower and upper terraces, respectively. In each

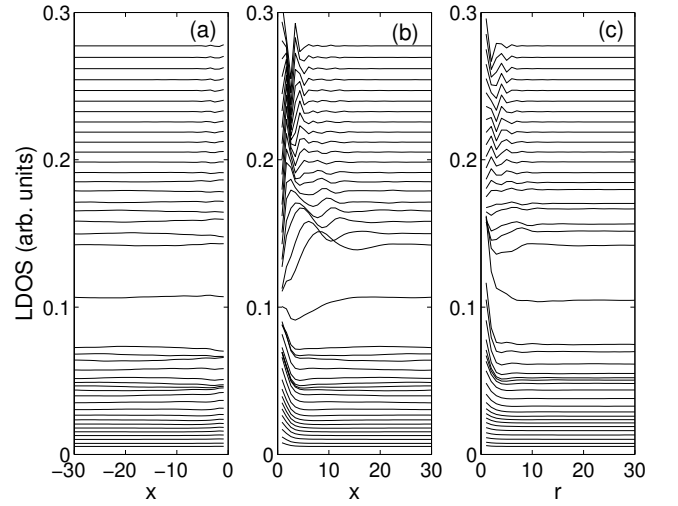


FIG. 3: LDOS as a function of the normal displacement  $x$  on the lower (a) and upper (b) terrace, and as a function of the radial distance  $r$  from a local impurity (c). In each panel the energy increases from  $! = 0$  at the bottom to  $! = 2$  at the top, with energy spacing  $! = 0.05$ . The arrows indicate the lines at  $! = 1$  which coincides with the bulk gap.

panel, the energy increases from  $! = 0$  at the bottom up to  $! = 2$  on the top, with energy interval  $! = 0.05$ . The arrow highlights the line with  $! = 1$ . For reasons to be clarified, we defined the origin of  $x$  differently for the two terraces. We observe that the oscillation of LDOS on the lower terrace is much weaker than that on the upper terrace. This important asymmetry can be checked experimentally, and can be understood as follows. As far as the LDOS (or the local Green's function) is concerned, the upper terrace can be obtained by setting  $m ! = 1$  on the left half of a surface. Therefore the upper terrace effectively experience a hard wall on the left. On the other hand, the lower terrace can be obtained by coupling a surface to an isolated upper-right layer through  $h_z$ . Thus the lower terrace effectively experiences a soft boundary on the right. The asymmetry clearly follows from the difference in the effective scattering mechanism, and makes it more sensible to define the origin of  $x$  as the boundary of such scattering in Figs.3 (a) and (b).

Let us concentrate on Fig.3 (b). Here the LDOS oscillation is negligibly small for  $! < 1$ , while more and more peaks appear significant for  $! > 1$ . The LDOS oscillation is a manifestation of quasiparticle scattering interference, [13] loosely referred to as the Friedel oscillation. [14] The wavelength  $\lambda$ , as is easily extracted from the first peak, should correspond to the wave number  $2k_{\parallel}$ , the characteristic momentum transfer during elastic quasiparticle scattering. Therefore  $k_{\parallel} = \lambda^{-1}$ . By this means we obtain a dispersion  $!$  vs.  $k_{\parallel}$ , which we plot in Fig.2 (e) (open squares). It clearly traces the outer border of the bulk continuum, and is therefore not related to the surface Dirac fermions. The lack of visi-

ble oscillations for  $\omega < 1$  is in nice agreement with the experiment [7, 8, 10]. The oscillation turns out to be more visible around a local impurity which we discuss in the next section.

#### IV. A LOCAL IMPURITY ON THE SURFACE

We consider a scalar impurity at the origin ( $r = 0$ ) on the surface with the potential matrix  $V_I$ , as illustrated in Fig. 1 (a). (Non-scalar impurities [15] can be discussed along the same line but we assume scalar ones are more likely to occur.) Given the unperturbed surface Green's function  $G$ , the perturbed Green's function  $G$  (in real space on the surface) can be obtained again by the T-matrix formalism,

$$G(r; r^0) = G(r - r^0) + G(r)TG(r - r^0); \quad (7)$$

where

$$G(r) = \frac{1}{M^2} \sum_{k,j,j'} G_{k,j,j'} e^{ik \cdot r}; \quad (8)$$

and  $T$  is given by  $T^{-1} = V^{-1}I - G(0)$ . The LDOS is given by

$$\rho(r) = \frac{1}{\pi} \text{Im Tr} G(r; r); \quad (9)$$

We set  $V = 1$  for a unitary impurity. The LDOS along a principle translation axis is plot in Fig. 3 (c). We see LDOS oscillation for  $\omega > 1$  similar to that in (b), although it is slightly weaker and has more complicated patterns. The oscillation below  $\omega = 1$  is still weak but the peaks are visible for  $\omega > 0.5$  and they shift toward the origin with increasing energy. To have a better idea of the wavelength, we plot the LDOS map in Figs. 4 for a few values of  $\omega$ . The view field bounded by  $26 \times 26$  is extracted from a  $400 \times 400$  surface. The oscillation, even if it is present, is beyond the view field for  $\omega < 0.4$ , while it is clear (from the dark rings) for higher energies. We extract the wave number  $2k_\parallel$  from the radii of the rings and plot  $\omega$  vs.  $k_\parallel$  in Fig. 2 (e) (open circles) for  $\omega < 1$ . It clearly follows the Dirac dispersion. For  $\omega > 1$ , the oscillation pattern is more complicated. In particular there are supermodulations for  $\omega = 1.2$  and  $\omega = 1.4$ , which can be understood from the double-ring structure in the corresponding map plot of the spectral function in Fig. 2 (d).

#### V. ANALYTICAL RESULTS FOR PURE DIRAC MODELS

**1D case:** For illustrative purpose and to set up notations, we start with the single-particle Hamiltonian in a 1D Dirac model, in the momentum space,  $h = k_\parallel \sigma_x$ , where

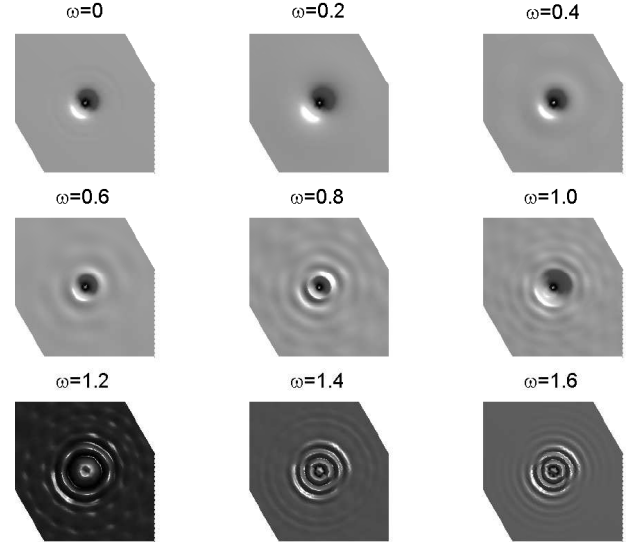


FIG. 4: Two-dimensional maps of the DOS near a local unitary impurity for specific values of  $\omega$ . The view field is bounded by  $26 \times 26$ . The strength scales with the darkness. The DOS at the origin vanishes in our case, but it is artificially reset to the value far from the impurity in order to enhance the contrast. Camera lighting is used.

$\sigma_n$  is one of the three Pauli matrices and the Dirac velocity is set to unity henceforth. The unperturbed Matsubara Green's function in the real space is given by

$$G(x) = \int \frac{dk}{2\pi} \frac{i\sigma_n \omega_0 + k \cdot \sigma_n}{i\omega_0 + k^2} e^{ikx} = i[\sigma_n \omega_0 + j \cdot \sigma_n \text{sign}(x)](x); \quad (10)$$

where  $\omega_0$  is the unitary matrix,  $\sigma_n$  is the Matsubara frequency, and we defined a kernel function

$$K(x) = \int \frac{dk}{2\pi} \frac{e^{ikx}}{i\omega_0 + k^2} = \frac{1}{2j\sigma_n j} e^{j\sigma_n x j}; \quad (11)$$

The on-site Green's function  $G(0) = i\sigma_n(0)\omega_0$  turns out to be a scalar. Suppose there is a local impurity potential  $V_0$  at the origin, the perturbed Green's function is conveniently obtained by the T-matrix formalism,

$$G(x; x^0) = G(0) + G(x)TG(x - x^0); \quad (12)$$

where  $T^{-1} = V^{-1}\omega_0 - G(0)$  is the inverse of the T-matrix. We will concentrate on  $g(x)$ , the trace of the change of the on-site Green's function as a function of  $x$ . Upon analytical continuation  $i\omega_0 \rightarrow \omega_0 + i0^+$ , its imaginary part gives the change of the LDOS. For  $x \neq 0$ , we find

$$g(x) = \text{Tr}[G(x)TG(x - x)] / \text{Tr}[(i\sigma_n \omega_0 + j\sigma_n j)(i\sigma_n \omega_0 - j\sigma_n j)] = 0; \quad (13)$$

Therefore right away from the impurity site, the LDOS is unaffected at all. Moreover, using the above T-matrix formalism it is easy to verify that the on-site Green's function  $G(x; x^0) = G(x - x^0)$  for  $xx^0 < 0$  in the limit  $V \rightarrow 1$ . This signifies perfect transmission (albeit with a phase lag of  $\pi$ ), a manifestation of the Klein Paradox. The mechanism behind this effect is the chirality (the alignment between the momentum and spin polarization) of the unperturbed eigen states. If an incoming state were scattered backward, energy conservation requires a flipping of the spin. But a scalar impurity can not flip the spin, so the scattering matrix element between these states vanishes identically.

For comparison, the retarded Green's function in 1D metal reads  $G(x) = \int \frac{dk}{2\pi} \frac{e^{ikx}}{i\epsilon - \epsilon(k) + i0^+}$  ( $k$  and  $v$  are the on-shell momentum and group velocity at real energy!). The oscillation can be worked out by the T-matrix approach again. It has a wave number  $2k_F$  and does not decay at all in the clean limit implicitly assumed. (In reality, the oscillation must decay beyond the mean free path.)

2D case: We write  $\mathbf{k} = k_x + q_y$  for 2D Dirac fermions. We first consider a domain wall with scalar potential  $V_0$  along the  $y$  direction. Then  $q$  is still a good quantum number. The scattering geometry is illustrated in Fig.5, where the circle of radius  $k_F$  is an energy shell, radial arrows indicate the momentum dependent spin polarization and the long thick arrow indicate a scattering process with incident angle  $\theta$  (so that  $q = k_F \sin \theta$ ). The  $q$ -resolved unperturbed Green's function is given by

$$G_q(x) = \int \frac{dk}{2\pi} \frac{e^{ikx}}{i\epsilon - \epsilon(k) + i0^+} = \frac{1}{2} \frac{e^{ipx}}{q^2 + k_F^2} e^{ipx} \text{sign}(x) \quad (14)$$

where we defined

$$q(x) = \frac{1}{2} \frac{e^{ipx}}{q^2 + k_F^2} \quad (15)$$

In particular,

$$G_q(0) = (i\epsilon_0 + q_y) q(0); \quad (16)$$

is no longer a scalar unless  $q = 0$ . The  $q$ -resolved perturbed Green's function is given by [12]

$$G_q(x; x^0) = G_q(x - x^0) + G_q(x) T_q G_q(x^0); \quad (17)$$

with

$$T_q^{-1} = V^{-1} - G_q(0); \quad (18)$$

By straightforward algebra, we find

$$\begin{aligned} g_1(x) &= \text{Tr}[G_q(x) T_q G_q(-x)] \\ &= \frac{4q^2 V_q^{-1}}{(i\epsilon_0 + V_q^{-1})^2 - q^2} q(2x); \end{aligned} \quad (19)$$

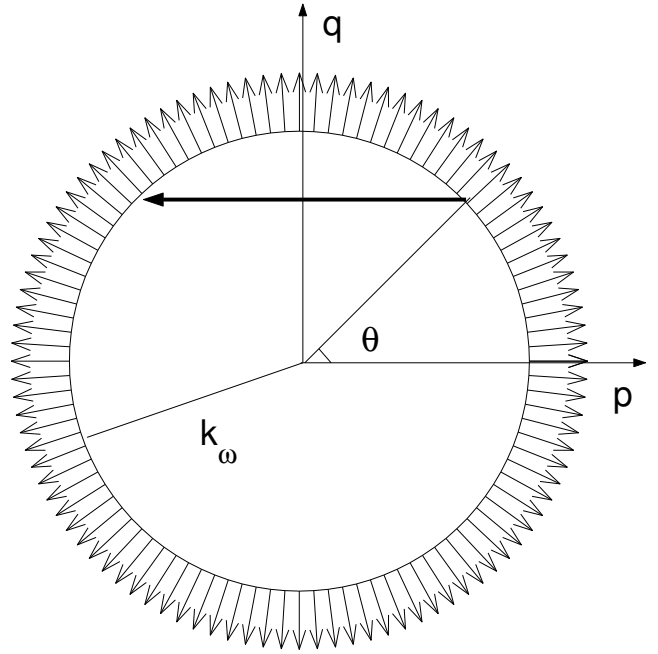


FIG. 5: Schematic plot of an energy shell at  $\epsilon$  with an on-shell momentum  $k_F$ . The radial arrows indicate the spin polarizations. The long thick arrow indicates a scattering process that conserves  $q$  in the case of a domain wall with its normal direction along the  $p$ -axis, and  $\theta$  is the incident angle.

where we defined  $V_q = V - q(0) = V - \frac{1}{2} \frac{e^{ipx}}{q^2 + k_F^2}$ .

Clearly the factor of  $q^2$  in  $g_1(x)$  follows from the requirement of spin overlap  $\sin^2$  during elastic scattering, as illustrated in Fig.(5). This leads to  $g_1(x) = 0$  for  $q = 0$  (normal incidence), recovering the 1D Klein paradox, as would have been anticipated. More importantly,  $g_1(x) \neq 0$  in the unitary limit  $V \rightarrow 1$  (a hard wall) for all values of  $q$ , and consequently in the real space  $g(x) = \int \frac{dq}{2\pi} g_1(x) = 0$  as long as  $|x| > 0$ . This explains nicely the numerical results in Sec.III for the terrace that the LDOS barely oscillates below the bulk gap energy. (In Sec.III we considered  $m \rightarrow 1$ , the effect of which is however identical to  $V \rightarrow 1$  here.) In the meantime, the on-site Green's function  $G_q(x; x^0) = G_q(x - x^0)$  for  $xx^0 < 0$  holds, signaling perfect transmission in analogue to the 1D case. This surprising result indicates that the Klein paradox also works in 2D but only for a hard wall.

For general strength of  $V$  (or soft walls), the asymptotic behavior in the limit of  $|j_n x| \rightarrow 1$  (where a saddle point approximation is valid) is given by

$$g(x) = \int \frac{dq}{2\pi} g_1(x) = \frac{V}{(2 + iV \text{sign}(\epsilon_0))^2} \frac{e^{ipx}}{|j_n x|} e^{2j_n x}; \quad (20)$$

where  $q = k_F \sin \theta$  is used. Upon analytical continuation  $j_n x \rightarrow i|$ , this amounts to an oscillation of LDOS with

an energy-dependent wave number  $2k_{\parallel} = 2j_{\parallel}j$  and an envelope function that decays as  $|x_j|^{-3/2}$ .

For comparison, in a 2D metal,  $G_q(x) = \int_{-\infty}^{\infty} \frac{e^{ik_{\parallel}x} \cos k_{\perp}x}{(2-j)^2} dk_{\parallel} = \frac{1}{(2-j)^2} \cos k_{\perp}x$  in real frequency. By the T-matrix formalism the domain wall leads to  $\frac{g(x)}{d} = \frac{e^{2ik_{\parallel}x} \cos k_{\perp}x}{(2-j)^2} = \frac{1}{(2-j)^2} \cos k_{\perp}x$  for  $k_{\parallel}x_j \ll 1$ . So the LDOS oscillation decays as  $|x_j|^{-1/2}$  near a domain wall in a 2D metal.[16] Notice that  $k_{\parallel} = 0$  is just the Fermi wave number.

For a point impurity in 2D, the unperturbed Green's function for Dirac fermions is given by

$$G(r) = \frac{1}{(2-j)^2} \frac{e^{ik_{\parallel}r}}{r^2} \quad (21)$$

where we find

$$G(r) = \frac{e^{j_{\parallel}r}}{4} \frac{1}{j_{\parallel}r} \quad (22)$$

in the asymptotic limit  $j_{\parallel}r \gg 1$ . For the on-site Green's function, a cutoff in momentum has to be introduced so that

$$G(0) = \frac{1}{4} \ln \frac{1}{j_{\parallel}^2} \quad (23)$$

Using the T-matrix formalism with  $T^{-1} = V^{-1} - G(0)$ , we find

$$g(r) = \text{Tr} G(r) T G(r) = \frac{1}{4} \frac{e^{2j_{\parallel}r}}{r^2} \quad (24)$$

to leading order in  $1/j_{\parallel}r$ . Upon analytical continuation, we see that the change of LDOS oscillates with an energy dependent wave number  $2k_{\parallel} = 2j_{\parallel}j$  and decays as  $r^{-2}$ . Notice that the oscillation exists even for  $V \ll 1$ , in contrast to the case of the domain wall. This is consistent with the results in Sec.IV. However, there is an important difference. Here a sharp resonance state appears at  $\epsilon = 0$  (in the unitary limit  $V \ll 1$ ) as seen from analytical continuation of  $g(r)$ , a well known result in many contexts.[17] This resonance state is absent in Sec.IV, as can be seen in Fig.3(b) or Figs.4. Qualitatively this is due to the fact that surface Dirac fermions are not completely confined on the surface. Depending on the planar momentum the wave function has varying extent of amplitude on the surface. Therefore the impurity is only partially seen by the surface Dirac fermions. Moreover, they exist only in a limited regime in the momentum space. An accurate discussion of these issues are left for future studies.

For comparison, in a 2D metal,  $G(r) = \int_{-\infty}^{\infty} \frac{e^{ik_{\parallel}r} \cos k_{\perp}r}{(2-j)^2} dk_{\parallel} = \frac{1}{(2-j)^2} \cos k_{\perp}r$  for  $k_{\parallel}r \ll 1$ .

By the T-matrix approach a local impurity leads to  $g(r) \propto G(r) \propto e^{2ik_{\parallel}r} / r^2$  for  $k_{\parallel}r \ll 1$ . So the LDOS oscillation decays as  $r^{-1}$  near a local impurity in a 2D metal.[16]

Similar analysis could be proceeded for 3D Dirac fermions in the presence of 2-, 1- and 0-dimensional impurities. As the impurity states would not be easily probed by STM, we do not go into detailed analysis. Some interesting behaviors are as follows. First, a 2D hard wall does not lead to any oscillation in LDOS away from the wall. For lower-dimension or general scalar impurities the oscillation is present, and decays faster than that for normal metals by a factor of  $1/r$ .

## V I. SUMMARY AND REMARKS

We analyze the behavior of surface states of topological insulators against local and extended impurities. Using an effective 3D lattice model we first obtain the spectral function of the surface states. This enables us to identify the contributions from massless Dirac fermions and bulk continuum. We then study the effects of a local impurity and a terrace on the surface. Away from a local impurity, the spatial oscillation in LDOS below the bulk gap is much weaker than that above. The LDOS oscillation is globally weak on the lower terrace. While on the upper terrace, the LDOS oscillation is barely visible below, in perfect agreement with the STM measurement, but it is significant above. The asymmetry of the LDOS oscillation on the lower and upper terraces is attributed to the difference in the effective scattering mechanism. From the LDOS oscillations we extract the modulation wave number  $2k_{\parallel}$  as a function of energy  $\epsilon$ . The dispersion ( $\epsilon$  vs.  $k_{\parallel}$ ) follows that of Dirac fermions for  $\epsilon < 0$ , but it follows the border of the bulk continuum for  $\epsilon > 0$ . The numerical results combine to reveal that the surface Dirac fermions are rather immune to the imperfections. We discuss such a behavior analytically by pure Dirac models. Because of a cancellation due to the alignment of momentum and spin polarization, the  $2k_{\parallel}$  oscillation in LDOS, if present, decays asymptotically faster by a factor of  $1/r$  than that for usual fermions. Specially, the oscillation is absent for a hard domain wall. Such behaviors are consistent with the 3d lattice model. We also find and discuss differences between surface and pure Dirac fermions.

Before closing, some remarks are in order. First, our simple model does not yield wavy energy shells (in the momentum space) for surface Dirac fermions due to warping terms, which would arise if longer-range hopping are considered. The warping term produces partial nesting and is responsible for some features in  $\text{Bi}_2\text{Te}_3$ . However, the merit of our simple model is it uncovers material-independent qualitative difference between surface Dirac fermions and bulk continuum. A material-

dependent calculation will be provided elsewhere. Second, we notice that a real terrace edge is not likely a straight line. This may be mapped to a straight edge but with excess in purities nearby. According to our results of both local in purity and terrace, a wiggling terrace edge should also lead to visible oscillations below the bulk gap, consistent with experiments.[9] Finally, in a model with multiple Dirac cones for the surface states, elastic scattering between cones is not suppressed by the chirality, and is therefore expected to induce visible LDOS oscillations even below the bulk gap.

While finalizing the writing of this work, we become aware of a related work using a 2D continuum model with warping terms.[18]

The work in Nanjing was supported by NSFC 10974086 and 10734120, the Ministry of Science and Technology of China (under the Grant No. 2006CB921802 and 2006CB601002) and the 111 Project (under the Grant No. B07026). The work in Hong Kong was supported by the RGC grant of Hong Kong.

---

E-mail address: xhwang@nju.edu.cn

- [1] L. Fu and C. L. Kane, Phys. Rev. B 76, 045302 (2007).
- [2] X. L. Qi, T. L. Hughes and S. C. Zhang, Phys. Rev. B 78, 195424 (2008); X. L. Qi, T. L. Hughes, S. Raghu, and S. C. Zhang, Phys. Rev. Lett. 102, 187001 (2009).
- [3] L. Fu, C. L. Kane, and E. J. Mele, Phys. Rev. Lett. 98, 106803 (2007); J. Moore and L. Balents, Phys. Rev. B 75, 121306 (2007); R. Roy, cond-mat/0604211.
- [4] H. J. Zhang et al, Nature Physics 5, 438 (2009).
- [5] Y. L. Chen, et al Science 325, 178-181 (2009); D. Hsieh, et al, Science 323, 919-922 (2009); D. Hsieh, et al, Nature 452, 970-974 (2008); H. J. Noh et al, Europhys. Lett. 81, 57006 (2008); Y. Xia, et al, cond-mat/0812.2078.
- [6] X. L. Qi, T. L. Hughes, and S. C. Zhang, Phys. Rev. B 78, 195424 (2008); X. L. Qi, R. D. Li, J. Zhang, and S. C. Zhang, Science 323, 1184-1187 (2009).
- [7] P. Roushan, J. Seo, C. V. Parker, Y. S. Hor, D. Hsieh, D. Qian, A. Richardella, M. Z. Hasan, R. J. Cava and Ali Yazdani, Nature 460 1106 (2009). absence of backscattering for helical fermions
- [8] Z. A. Pichshev, et al, arxiv:0908.0371.
- [9] T. Zhang, et al, arXiv:0908.4136.
- [10] K. K. Gomes, W. Ko, W. M. Ma, Y. Chen, Z.-X. Shen, H. C. Manoharan, arXiv:0909.0921.
- [11] Q. K. Xue, private communications.
- [12] Qiang-Hua Wang and Z. D. Wang, Phys. Rev. B 69, 092502 (2004).
- [13] Qiang-Hua Wang and Dung-Hai Lee, Phys. Rev. B 67, 020511 (2003); J. E. Hoffman, et al, Science 297, 1148 (2002); K. McElroy, et al, Nature 422, 592 (2003).
- [14] J. Freidel, Nuovo Cimento Suppl. 2, 287 (1958).
- [15] Q. Li, et al, Phys. Rev. Lett. 102, 156603 (2009).
- [16] M. F. Crommie, C. P. Lutz, and M. Eigler, Nature 363, 524 (1993).
- [17] M. I. Salkola, A. V. Balatsky, and D. J. Scalapino, Phys. Rev. Lett. 77, 1841 (1996); Qiang-Hua Wang, Phys. Rev. Lett. 88, 057002 (2002); V. M. Pereira, et al, Phys. Rev. Lett. 96, 036801 (2006).
- [18] Xiaoting Zhou, Chen Fang, Wei-Feng Tsai, and Jiang-Ping Hu, cond-mat/0910.0756.